Micromagnetic models of pseudo-single domain grains of magnetite near the Verwey Transition

JOURNAL OF GEOPHYSICAL RESEARCH, VOL. 104, NO. B12, PAGES 29,203–29,217, DECEMBER 10, 1999

Micromagnetic models of pseudo-single domain grains of magnetite near the Verwey Transition

A. R. Muxworthy[1]

Department of Earth Sciences, University of Oxford, Oxford, England

W. Williams

Department of Geology and Geophysics, University of Edinburgh, Edinburgh, Scotland

Abstract. Domain structures of small pseudo-single domain (PSD) magnetite near the Verwey transition (T_v) at ≈120 K were modeled using an unconstrained three-dimensional micromagnetic algorithm. The single-domain (SD) threshold (d_o) for the monoclinic phase below T_v was calculated to be ≈0.14 μm at 110 K. However, it is postulated that as a result of the very high energy barriers in the monoclinic phase, grains near d_o in size and in vortex states are unlikely to denucleate domain walls to become SD. Low-temperature cycling of saturation isothermal remanence (SIRM), thermoremanence (TRM), and partial TRM (pTRM) through T_v was simulated. Domain structures were found to align along the monoclinic "easy" magnetocrystalline anisotropy axis, i.e., the c axis, on simulated cooling through T_v. This process was found to "destroy" SIRM structures giving rise to demagnetization; however, for TRM and pTRM structures only "closure" domains were removed increasing magnetostatic leakage giving rise to a reversible anomaly in rough agreement with experimental studies. SIRM displayed a smaller anomaly at T_v, in agreement with experimental studies.

1. Introduction

Magnetite undergoes a phase transition at 120-124 K called the Verwey transition, T_v [*Verwey*, 1939], while at 130 K the first cubic-magnetocrystalline anisotropy constant (K_1) passes through an isotropic point T_k [*Bickford et al.*, 1957]. On zero-field cooling of rocks to temperatures below T_v the magnetic remanence carried by multidomain (MD) magnetite grains partially demagnetizes leaving a relatively stable remanence [*Heider et al.*, 1992; *McClelland and Shcherbakov*, 1995]. The nature and origin of this stable, low-temperature demagnetized remanence are of great interest to paleomagnetists because isolated hard magnetic remanences have been associated with primary remanences [*Ozima et al.*, 1964; *Kobayashi and Fuller*, 1968].

Previous attempts to understand the demagnetization processes during cooling have been purely experimental, usually consisting of measuring the behavior of saturation isothermal remanence (SIRM) induced at room temperature, during low-temperature cycling in zero field [e.g., *Kobayashi and Fuller*, 1968; *Hodych*, 1991; *Halgedahl and Jarrard*, 1995; *Hodych et al.*, 1998]. These studies have found that remanence decreases on cooling to T_k and T_v, and it has been concluded that low-temperature demagnetization (LTD) is due to $K_1 \rightarrow 0$ at T_k. However, the first extensive series of measurements of low-temperature cooling of thermoremanences (both full thermoremanence (TRM) and partial TRM (pTRM)) for randomly orientated assemblages of hydrothermal pseudo-single-domain (PSD) and MD magnetite crystals [*Muxworthy*, 1998; *Muxworthy and McClelland*, 1999a] have found the behavior of thermoremanence to be different from that of SIRM. Thermoremanences displayed large discontinuities on cooling through T_v, i.e., the thermoremanences display reversible positive anomalies on cooling through T_v. Clearly, a new interpretation and model for LTD is required. *Muxworthy and McClelland* [1999a] explain the discontinuity at T_v in terms of metastable and unstable domain structures. However, their interpretation is far from rigorous, and no analytical formulation was made.

Other attempts to resolve domain behavior at T_v have been limited. *Moloni et al.* [1996] have reported the only direct observations of the domain structure in

[1]Now at Institut für Allgemeine und Angewandte Geophysik, Universität München, Munich, Germany.

Paper number 1999JB900294.
0148-0227/99/1999JB900294$09.00

low-temperature phase of magnetite. However, *Moloni et al.* [1996] were unable to observe domain structure above 111 K and therefore were unable to directly observe domain structures on cooling through T_k and T_v.

As experimental evidence has not elucidated the low-temperature behavior of the domain structure, it seemed suitable to investigate the low-temperature structure using three-dimensional micromagnetic modeling with an implemented fast Fourier transform (FFT) algorithm [*Wright et al.*, 1997]. In this paper the low-temperature phase of magnetite is investigated and the low-temperature cooling experiments of different initial remanences, e.g., SIRM TRM and pTRM, simulated.

2. Brief Review of the Verwey Transition

The Verwey transition has recently been extensively reviewed from a rock magnetic perspective [*Dunlop and Özdemir*, 1997; *Muxworthy and McClelland*, 1999b]; here only a brief summary is given. On cooling through T_v, magnetite's crystallographic structure changes from cubic above T_v to a monoclinic structure on cooling through T_v [*Otsuka and Sato*, 1986]. The relationship between the cubic axis phase ([100], [010], [001]) and monoclinic phase axis (a, b, c) is shown in Figure 1. At T_v there is a sharp reduction in electron mobility which causes a large increase in the magnetocrystalline anisotropy [*Abe et al.*, 1976; *Belov*, 1993](Figure 2). There are also significant anomalies in the magnetostrictive anisotropy constants [*Tsuya et al.*, 1977]. There is also a small anomaly in the spontaneous magnetization (M_s) [*Belov*, 1993; *Muxworthy and McClelland*, 1999b], which can be explained in terms of the magnetoelectronic model of the Verwey transition [*Belov*, 1993].

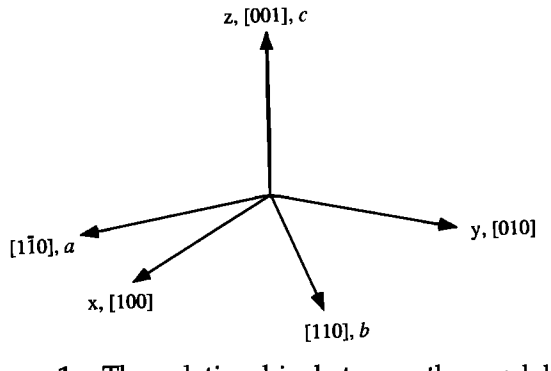

Figure 1. The relationship between the model axis (x,y,z), cubic phase axis ([$\bar{1}$00],[010],[001]) and monoclinic phase axis (a,b,c). In the cubic phase the [111] (and [$\bar{1}$11], [1$\bar{1}$1], [11$\bar{1}$] *etc.*) is the easy axis above 130 K, and the [100] (and [$\bar{1}$00], [001], [0$\bar{1}$1] *etc.*) between T_v and 130 K. In the monoclinic phase the c-axis is the easy direction, yet the a-axis is much harder than the b-axis.

3. Discrete Micromagnetic Model

The basic algorithm used to model the results in this paper was fully described by *Wright et al.* [1997]. Here a only a brief description of the algorithm and the changes made to accommodate the low-temperature phase are given. To simulate low-temperature cycling of thermoremanences, it was necessary to include the temperature dependency of the various parameters between 70 K and T_c (851 K).

The model subdivides the cubic grain of length d into a number (n) of finite element subcubes of length Δ, which are assumed to be homogeneously magnetized. All the subcubes have equal magnetic magnitude, but their magnetization can vary in direction. The domain structure is calculated by optimizing the total free magnetic energy (E_{tot}), which is the sum of the exchange energy E_{ex}, the external field energy E_h, the magnetostatic energy E_d, and the anisotropy E_{anis} [*Williams and Dunlop*, 1989; *Wright et al.*, 1997]. For all temperatures in the model E_h, E_{ex}, and E_d are given by

$$E_h = -\mu_0 M_s \sum_{i=1}^{n} \mathbf{H_e} \cdot m_i \Delta^3, \quad (1)$$

$$E_{\text{ex}} = A \sum_{i=1}^{n} (\nabla m)_i^2 \Delta^3, \quad (2)$$

$$E_d = -\frac{\mu_0 M_s}{2} \sum_{i=1}^{n} \mathbf{H_{d,}}_i \cdot m_i \Delta^3, \quad (3)$$

where $\mathbf{H_e}$ is the external field with magnitude H and direction ϕ_H and θ_H, μ_0 is the permeability of free space, A is the exchange constant, and $\mathbf{H_{d,}}_i$ is the magnetic field at the location m_i due to each magnetic dipole in the system.

Above room temperature, $A(T)$ was taken to vary as $M_s^{1.7}(T)$ [*Heider and Williams*, 1988]. Below room temperature, there are no reported measurements leading directly to the calculation of $A(T)$. However, $A(T)$ is proportional to the exchange integral [*Dunlop and Özdemir*, 1997], which does not vary significantly from the room temperature value on cooling to below T_v [e.g., *Torrie*, 1967]. In this simplified model it was therefore assumed that $A(T)$ did not vary below room temperature. The temperature dependence of M_s was taken from *Pauthenet and Bochirol* [1951] for $T > 273$ K and from *Belov* [1993] for $T \leq 273$ K.

3.1. Anisotropy Energy

E_{anis} is the sum of the magnetocrystalline, magnetostrictive and magnetoelastic anisotropy energies [*Kittel*, 1949; *Ye et al.*, 1994]. For reference, the magnetostrictive anisotropy is a second-order effect due to the interaction of the magnetocrystalline energy and elastic energies, causing spontaneous deformation if

this reduces the total energy [*Kittel*, 1949]. The magnetoelastic anisotropy energy is the anisotropy induced if the magnetic material is subjected to either external or internal stresses.

3.1.1. Magnetocrystalline anisotropy. In this model the magnetocrystalline anisotropy energy is split into the high-temperature cubic phase (E_k^c) and a low-temperature monoclinic phase (E_k^m), given by equations (4) and (5) of *Muxworthy and McClelland* [1999b]. After considering Figures 11 and 13–16 of *Muxworthy and McClelland* [1999b], it is possible to simplify the two expressions for E_k^c and E_k^m, which in terms of the discrete model are given by

$$E_k^c = \sum_{i=1}^{n} [K_1(\alpha_1^2\alpha_2^2 + \alpha_2^2\alpha_3^2 + \alpha_1^2\alpha_3^2)]\Delta^3, \quad (4)$$

$$E_k^m = \sum_{i=1}^{n} [\mathcal{K}_a\alpha_a^2 + \mathcal{K}_b\alpha_b^2 - \mathcal{K}_u\alpha_{111}^2]\Delta^3, \quad (5)$$

where $\mathcal{K}_i$ are the monoclinic magnetocrystalline, $\alpha_{1,2,3}$ and α_{111} are the directional cosines of the magnetization vector with respect to the [111] cubic axes, and α_a, α_b are the directional cosines of the magnetization with respect to the monoclinic a, b axes, respectfully. *Abe et al.* [1976] added the $-\mathcal{K}_u\alpha_{111}^2$ term to accommodate for the small rhombohedral distortion. The temperature dependence of the magnetocrystalline constants used in the model are shown in Figure 2 for $T \leq 273$ K. Above 273 K, the temperature dependence of K_1 was taken from *Fletcher and O'Reilly* [1974]. It should be noted that the magnetocrystalline anisotropy "constants" in Figure 2 are not strictly $K_1, \mathcal{K}_i$ but $K_1', \mathcal{K}_i'$, i.e., $K_1, \mathcal{K}_i$ plus a magnetostrictive contribution [*Ye et al.*, 1994]. However, this magnetostrictive contribution is not the magnetostrictive anisotropy energy and should be treated as a small error.

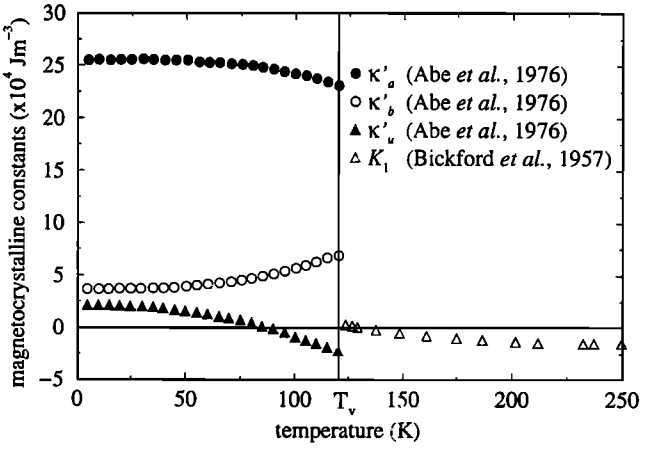

Figure 2. Temperature dependence of the magnetocrystalline constants used in the model; $\mathcal{K}_i$ are the monoclinic constants, and K_1 is the cubic constant.

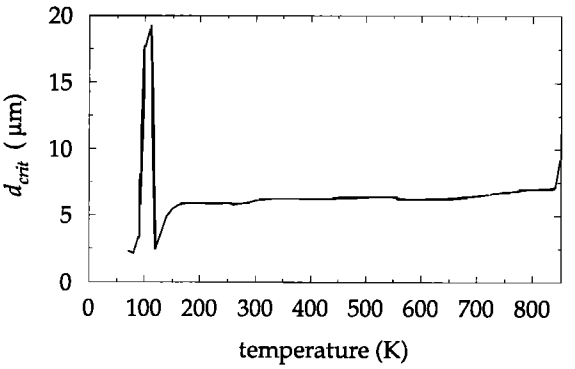

Figure 3. d_{crit} plotted as a function of temperature using equation 6. Above the line the magnetostrictive self-energy starts to dominate.

3.1.2. Magnetostrictive anisotropy. This term was not included in the model because there are as yet unresolved technical difficulties in incorporating it for spatially independent crystals, i.e., single crystals. *Fabian and Heider* [1996] have managed to incorporate it in an elastically infinite medium; however, this can lead to an an overestimation of the elastic properties. The significance of its omission can be estimated by considering the characteristic sample size (d_{crit}) above which the magnetostrictive term is thought to dominate the domain structure. Here d_{crit} is given by [*Fabian et al.*, 1996]

$$d_{\text{crit}} = \frac{8\sqrt{A|K_1, \mathcal{K}_a|}}{c_{44}\lambda_{111}^2} \quad (6)$$

where c_{44} is an elastic modulus and λ_{111} is the cubic magnetostriction anisotropy constant for the [111] crystallographic direction. The d_{crit} is calculated as a function of temperature (Figure 3). The thermal behavior of the constants were taken from; *Heider and Williams* [1988], *Abe et al.* [1976], *Fletcher and O'Reilly* [1974], *Moskowitz* [1993], and *Tsuya et al.* [1977]. As stated above, A is assumed to be constant below room temperature, and c_{44} is assumed to be constant for all temperatures. It is seen in Figure 3 that nowhere in the temperature range of interest does d_{crit} fall significantly below the maximum grain size modeled in this study, i.e., 0.6 μm. Therefore, in this simplified model it can be assumed that the omission of the magnetostrictive anisotropy was not significant.

3.1.3. Magnetoelastic anisotropy. The models in this simplified study were for stress free samples, i.e., no dislocations and no external stress, making the contribution from the magnetoelastic anisotropy zero.

3.2. Total Magnetic Energy

The magnetic anisotropy energy is simply represented by E_k, and the total magnetic energy (E_{tot}) given by

$$E_{tot} = E_{ex} + E_h + E_d + E_k. \quad (7)$$

The domain state of grain is calculated by optimizing E_{tot} by the conjugate-gradient method, to give the local energy minimum (LEM). The magnetization in each sub-cube represents the averaged magnetization direction of many hundreds of atomic magnetic dipole moments for which it is assumed that the magnetization is continuous. This effectively puts a lower limit on the resolution of the model; $\Delta \geq 0.005$ μm [*Williams and Wright*, 1998]. However, *Williams and Wright* [1998] propose that as long as domain walls are represented by approximately four or more subcubes, then the results still reflect the general domain structure.

The model does not include the effect of thermal fluctuations, which are thought to be important in determining the domain structure at high temperatures [*Dunlop and Özdemir*, 1997]. Attempts have been made to incorporate a thermal fluctuation approximation [*Thomson et al.*, 1994], though this addition consumes vast amounts of CPU time. This study was primarily concerned with the magnetic behavior below room temperature, where the importance of thermal fluctuations is greatly reduced. The only error may arise in the simulation of thermoremanences; however, it was not the intention of the present study to accurately model the acquisition of thermoremanences, and the simulated thermoremanences should only be treated as approximations.

4. Domain Structure in the Monoclinic Phase of Magnetite Near the SD/MD Transition

In this section the domain structures of small cubic grains of magnetite in the monoclinic phase are examined, and the single-domain (SD)/MD boundary is calculated. The large increase in the magnetocrystalline anisotropy on cooling through T_v (Figure 2) should be expected to effect the critical SD size d_o. There are traditionally two approaches for estimating d_o; first, by considering where the domain wall thickness approaches d_o [*Néel*, 1947] and, second, by calculating where the energies for single-domain and two-domain structures are equal [*Kittel*, 1949]. The former gives the relationship $d_o \propto \sqrt{1/K_u}$, while the later finds $d_o \propto \sqrt{K_u}$, where K_u is the uniaxial anisotropy. Obviously, these two results are contradictory. Néel's criterion appears to be more realistic for the cubic phase because the two-domain structure used in the Kittel approximation does not exist in micromagnetic solutions. Micromagnetic models for the cubic phase predict a SD $\leftrightarrow$ vortex structural transition [*Fabian et al.*, 1996; *Williams and Wright*, 1998]. However, micromagnetic models calculate d_o by minimizing the energy, in a manner similar to Kittel's criteria.

Using Néel's criterion to compare the monoclinic critical domain size d_o^m at 100 K with the cubic critical domain size d_o^c at 300 K gives $d_o^m \approx [K_1(300\text{ K})/K_i(100\text{ K})]^{1/2} d_o^c \approx 0.25 d_o^c$. Taking d_o^c to be $\approx 0.07\mu$m at room temperature [*Williams and Wright*, 1998] gives an estimate for $d_o^m \approx 0.02$ μm. Similarly, using Kittel's criterion gives $d_o^m \approx 4d_o^c \approx 0.28$ μm.

4.1. Stability of Domain Structure in the Monoclinic Phase of Magnetite and Calculation of d_o^m

It was initially intended to calculate the monoclinic SD critical size using a simple procedure described by *Fabian et al.* [1996] and *Williams and Wright* [1998]; that is, simply starting with an initial SD/flower state, the grain dimension is increased until a vortex state forms. This is then repeated in reverse, decreasing the grain size until a SD/flower state is energetically favorable. However, on application to the monoclinic phase, this approach proved to be unsuccessful because the energy barrier between the SD and vortex/two-domain state is too high for an unconstrained transition to occur, even for very large/small grain sizes.

Instead, a constrained model, similar to that described by *Enkin and Williams* [1994] was used to examine the critical SD grain size. Working with a resolution of $7 \times 7 \times 7$, *Enkin and Williams* [1994] constrained two groups of four cells on the top and bottom, i.e., the $z = 1$ ($\Phi_{z=1}$) and $z = 7$ ($\Phi_{z=7}$) planes, which were rotated through 360°at some step interval, usually 10-15°. For each angle of $\Phi_{z=1}$ and $\Phi_{z=7}$ the total energy of the domain is minimized with respect to the other cells, and an energy surface is plotted for the two degrees of freedom.

In the monoclinic phase, constraining cells in the z plane forces the alignment of the constrained cells to the energetically unfavorable a axis. To avoid this, cells were constrained in the y plane ($\Phi_{y=1}$ and $\Phi_{y=7}$) (the x plane would have equally sufficed). Unfortunately, owing to the high-energy barriers in the monoclinic phase, it was necessary to constrain 16 cells in each group for the domain structure to display uni-

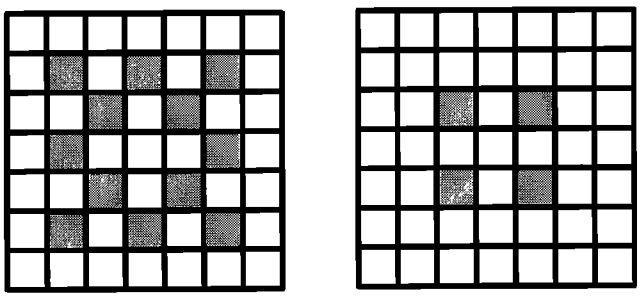

Figure 4. Schematic diagram showing the positioning of the constrained cells. The two groups of cells, *i.e.*, $y = 1$ and 2 and $y = 6$ and 7 are constrained to the angles $\Phi_{y=1}$ and $\Phi_{y=7}$ and are rotated through 360° in the y-plane.

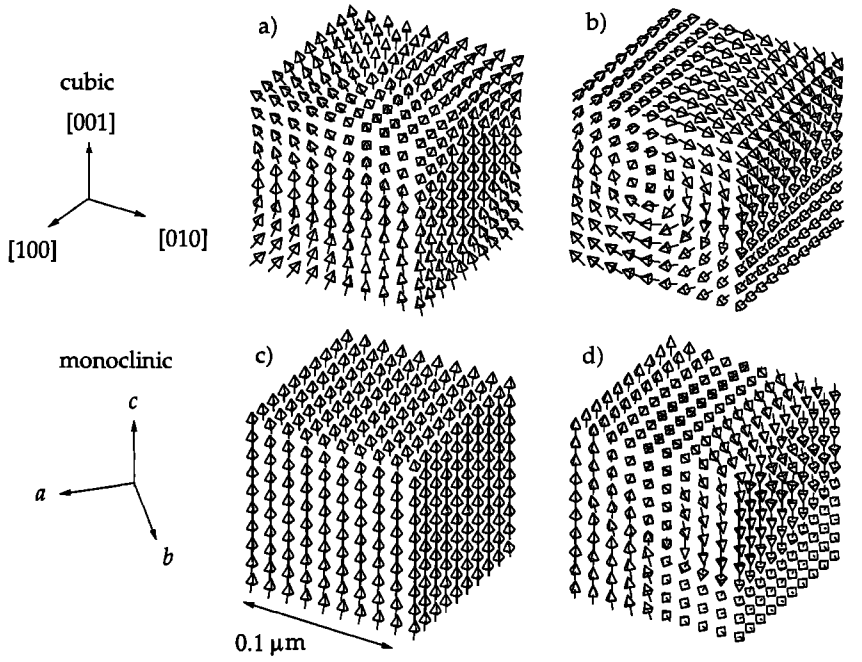

Figure 5. The two types of LEM states that can exist for cubic grains of size 0.10 μm in both the cubic phase (a & b) and the monoclinic phase (c & d). For the cubic phase at 300 K a) flower state, where the magnetization flowers out at the grain surface, and b) vortex tate, where the magnetization curls around a central core. In the monoclinic phase at 110 K the SD/flower state (c) has greatly reduced flowering, and the two-domain/vortex state (d) has reduced curl compared to the cubic phase vortex state. The monoclinic vortex phase resembles Kittel's (1949) "classical" two domain structure [Figure 6].

form behavior. The layout of the constrained cells in the four planes $y = 1$ ($\Phi_{y=1}$), $y = 2$ ($\Phi_{y=1}$), $y = 6$ ($\Phi_{y=6}$), and $y = 7$ ($\Phi_{y=7}$), is shown in Figure 4. This represents 9.3% of the total number of cells within the $7 \times 7 \times 7$ model, which is approximately the upper limit for this type of constrained model.

Using this constrained approach, it was found that there are two basic stable LEM states available to the magnetite cubes smaller than 0.3 μm at 110 K; either a single-domain/flower domain (Figure 5c) or two-domain/vortex state structures (Figure 5d). On comparison with similar cubic phase structures (Figures 5a and 5d), the large increase in the magnetocrystalline anisotropy on cooling through T_v (Figure 2), is seen to rotate the domain structure toward the z direction, i.e., the "easy" magnetocrystalline direction (Figure 1). This reduces the flowering in the SD-like state (compare Figures 5a and 5c), and the monoclinic vortex is closer in appearance to Kittel's "classical" two-domain structure without closure domains (compare Figures 5b, 5d and 6). This is to be expected if the relative anisotropy, Q, is considered, where $Q = 2K_u/\mu_0 M_s^2$ [*Rave et al.*, 1998]. For small values of Q, vortex states are favorable over Kittel-like two-domain states (Figure 6); however, if $Q \geq 1$, then two-domain states are more favorable [*Rave et al.*, 1998]. Assuming that below T_v, $K_a, \approx K_u$ and above T_v, $K_1 \approx K_u$, Q can be plotted as a function of temperature (Figure 7). Above T_v, $Q \leq 1$; however, below T_v, $Q \geq 1$, suggesting that the vortex state is unfavorable [*Rave et al.*, 1998].

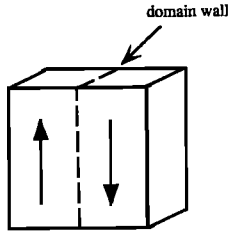

Figure 6. Kittel's (1949) "classical" model of a two domain grain without closure domains.

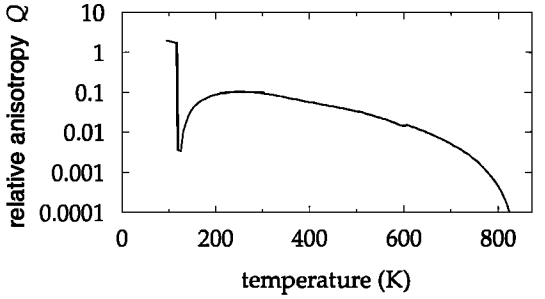

Figure 7. Relative anisotropy Q as a function of temperature for magnetite. The anomalous behavior at $\approx$ 120 K is due to the Verwey transition.

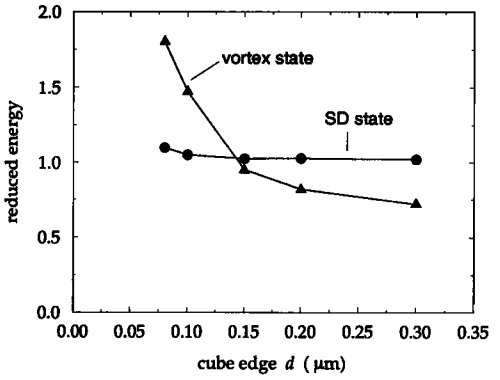

Figure 8. The reduced energy of LEM states as a function of grain size at 110 K, where the reduced energy is the total energy normalized by the energy of a cube uniformly magnetized along the easy axis. The line marked "SD" corresponds to the SD/flower state, and the line marked "vortex" corresponds to the vortex/2-domain LEM state. The critical size of a transition from single domain [Figure 5c] to 2 domain/vortex structure [Figure 5d], occurs at ≈ 0.14 μm. Because of the high energy barriers between the two possible states there is a wide range of grain sizes over which the two domain states can co-exist.

Figure 8 shows the energy for the two possible LEM states for the monoclinic phase of magnetite at 110 K as a function of grain size. Energy surfaces at 110 K for grain sizes 0.1 to 0.2 μm are shown in Figure 9. The energy surfaces correspond to the domain structure after minimization of the unconstrained cells. As a comparison the energy surface for a 0.06 μm cube of magnetite at 300 K, i.e., below d_o^c in the cubic phase, is shown in Figure 10. Figure 10 compares well with identical energy surfaces published by *Enkin and Williams* [1994].

The monoclinic phase has LEM SD states at $\Phi_{y=1} = 0°$, $\Phi_{y=7} = 0°$, and the cubic phase at $\Phi_{y=1} = 45°$, $\Phi_{y=7} = 45°$, and there are similar differences for the orientation of the vortex LEM states (Figure 9). This is due to the preferred magnetocrystalline anisotropy easy axis in the cubic and monoclinic phase.

For a grain of dimension 0.1 μm at 110 K the SD/flower state is energetically the most favorable; however, on increasing the grain size to 0.15 μm the two-domain/vortex state is slightly more favorable, and on increasing to 0.2 μm its energy decreases further (Figures 8 and 9). The transition from SD ↔ two-domain/vortex occurs at ≈ 0.14 μm and is much closer to the Kittel's estimate of 0.28 μm, than to Néel's of 0.02 μm. This maybe attributed to the SD and two-domain/vortex structures in the monoclinic phase which are closer in appearance to the "classic domain" structures described by *Kittel* [1949] (Figure 6).

In the monoclinic phase the energy barriers to be surmounted on swapping between antiparallel SD/flower states or between SD/flower states and two-domain/vortex states are larger than those found in comparable structures in the cubic phase of magnetite; for example, in the cubic phase the maximum reduced energy barrier to be overcome is ≈0.2, while in the monoclinic phase the barrier increases to ≈1.1 (Figures 9 and 10). The high-energy barriers in the monoclinic phase means that it is unlikely that grains in the size range 0.07-0.14 μm already in vortex states will denucleate domain walls to become SD. These high-energy barriers are reflected by the large coercive forces measured for the monoclinic phase [e.g., *Schmidbauer and Keller*, 1996].

4.2. Orientation of Magnetic Moments in Vortex Structures in the Monoclinic Phase

On cooling through T_v, the large increase in intensity of the magnetocrystalline anisotropy and the reduction in symmetry cause the the magnetic moments to align in the *a* plane at all times, even in domain walls and in the center of vortex structures. For example, in the cubic phase at room temperature the surface moments of a vortex structure in a 0.1 μm grain align along the direction of the grain boundaries (Figure 11a); however, on cooling to below the Verwey transition the surface moments rotate into the *a* plane, i.e., away from the hard *a* axis (Figure 11b).

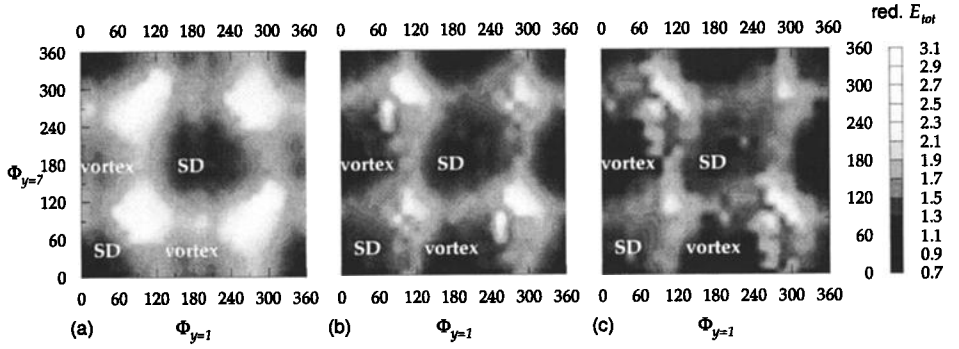

Figure 9. Energy surfaces for a) 0.10 μm, b) 0.15 μm and c) 0.2 μm cubes of magnetite in the monoclinic phase at 110 K. The favorable SD ($\Phi_{y=1} = \Phi_{y=7}$) and vortex ($\Phi_{y=1} = 180° + \Phi_{y=7}$) states are marked. Favorable vortex/2-domain structures and SD structures are marked. The model resolution was 7 × 7 × 7.

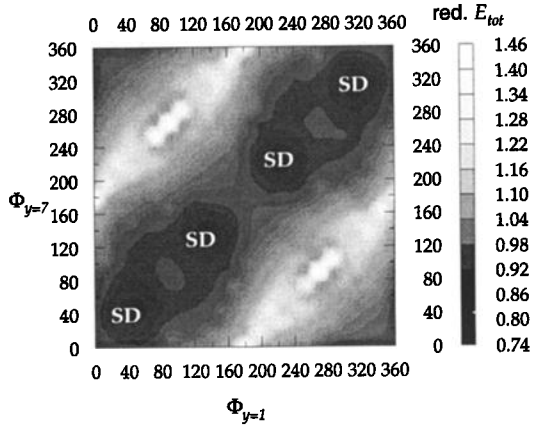

Figure 10. Energy surfaces for 0.06 μm cube of magnetite in the cubic phase at 300 K. 0.06 μm is just below the d_o^c ($\approx$ 0.07 μm). The LEM potential wells are much shallower than those observed for the monoclinic magnetite grains of similar sizes, *cf.* Figure 9. The favorable SD states are marked. The model resolution was of 7 × 7 × 7.

5. Simulated Low-Temperature Cycling of Remanences

The behavior of different kinds of remanences (SIRM and TRM) to low-temperature cycling was modeled in grains in the size range 0.1–0.6 μm. The importance of the initial orientation of remanence during low-temperature cycling was considered by simulating room temperature SIRM in two different directions, i.e., in the direction of the x axis (SIRM$_x$) and z axis (SIRM$_z$). The SIRMs were modeled by optimizing the domain structure in field of 2 T, followed by optimization of the same domain structure in zero field at the same temperature. To simulate the low-temperature cycling, the domain structure was optimized at 20 K intervals in zero field down to 150 K and then in smaller steps to 70 K with domain structure optimization as frequent as 2 K near T_v. On subsequent simulated warming, the temperature steps were reversed. Low-temperature cycling of TRM was modeled in a similar manner to SIRM; that is, the domain structure was optimized at regular temperature intervals during simulated cooling from T_c to 70 K, with a field (H = 100 μT) applied between appropriate temperatures.

Two types of TRM were induced: type 1, samples are cooled from above T_c to T_2 in a field, where room temperature, rtp $\leq T_2 < T_c$ ($T_c \downarrow T_2$, H=on; pTRM$^{T_c}_{T_2}$), and type 2 pTRM acquired by cooling from T_c to a temperature T_1 in zero field and from T_1 to T_2 in a field, where rtp $\leq T_2 < T_1 < T_c$ ($T_c \downarrow T_1$, H = off; $T_1 \downarrow T_2$, H=on; pTRM$^{T_1}_{T_2}$). In both cases the inducing field $\mathbf{H_e}$ was in the x axis direction with an intensity of 100 μT. Owing to the importance of thermal history on the magnetic behavior of the remanence [*Vinogradov and Markov*, 1989], type 2 thermoremanences were "cooled" from T_c in zero field. Below T_2, $\mathbf{H_e}$ was set to zero. The 0.1 μm cubes were modelled using a 20 × 20 × 20 resolution, and the 0.3 μm and 0.6 μm cubes were modeled with a resolution of 30 × 30 × 30.

5.1. Solutions for SIRM$_x$ and SIRM$_z$

5.1.1. The 0.1 μm cubic grains. The initial room temperature SIRM domain structure for 0.1 μm cubes of magnetite is a flower state, with the moment aligned

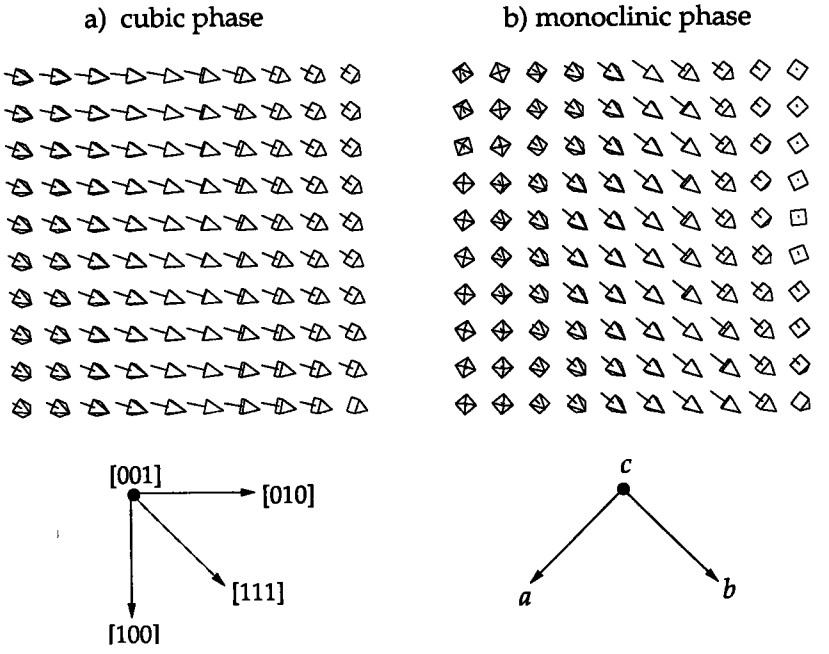

Figure 11. The surface z-plane of vortex structure in a 0.1 μm grain at a resolution of 10 × 10 × 10 in a) cubic phase (300 K) and b) monoclinic (110 K). In the monoclinic phase the domain walls are orientated away from the a-axis towards the b-axis.

Table 1. Intensity and Direction of Reduced $SIRM_x$ and $SIRM_z$ During Simulated Low-Temperature Cycling for Three Grain Sizes

Treatment	0.1 μm		0.3 μm		0.6 μm	
	M/M_{SD}	θ, ϕ	M/M_{SD}	θ, ϕ	M/M_{SD}	θ, ϕ
			$SIRM_x$			
Initial	0.92	90°, 0°	0.09	92°, 355°	0.01	90°, 5°
Monoclinic	0.96	8°, 224°	0.25	54°, 355°	0.27	44°, 359°
Memory	0.92	3°, 225°	0.04	95°, 6°	0.01	76°, 357°
			$SIRM_z$			
Initial	0.92	0°, 0°	0.17	5°, 1°	0.01	0°, 347°
Monoclinic	0.94	3°, 1°	0.24	24°, 191°	0.06	37°, 166°
Memory	0.92	1°, 1°	0.01	6°,198°	0.01	2°, 165°

Initial is the reduced SIRM at 270 K before simulated cooling, monoclinic the reduced SIRM at 117 K in the monoclinic phase of magnetite after simulated cooling from room temperature, and memory is the reduced SIRM remaining at 270 K after simulated low-temperature cycling.

in the direction of the applied field. $SIRM_x$ and $SIRM_z$ are identical apart from orientation, with a reduced remanent magnetization at 270 K of 0.92% (Table 1). The reduced magnetization is the magnetization (M) normalized by the magnetization of a cube uniformly magnetized along the easy axis (M_{SD}). On cooling through the Verwey transition the domain structure of the $SIRM_z$ remains aligned in the z axis; however, the entire domain structure of the $SIRM_x$ rotates to align 8° from the z axis. The small horizontal component of the $SIRM_x$ moment is aligned at an angle $\phi = 224°$, i.e., in the direction of the monoclinic b axis (Figure 1). In both cases there is a reduction in flowering (Table 1). On warming to room temperature, $SIRM_x$ rotates further toward the z axis, reducing the offset to < 3°. The degree of flowering returns to its initial value of 0.92

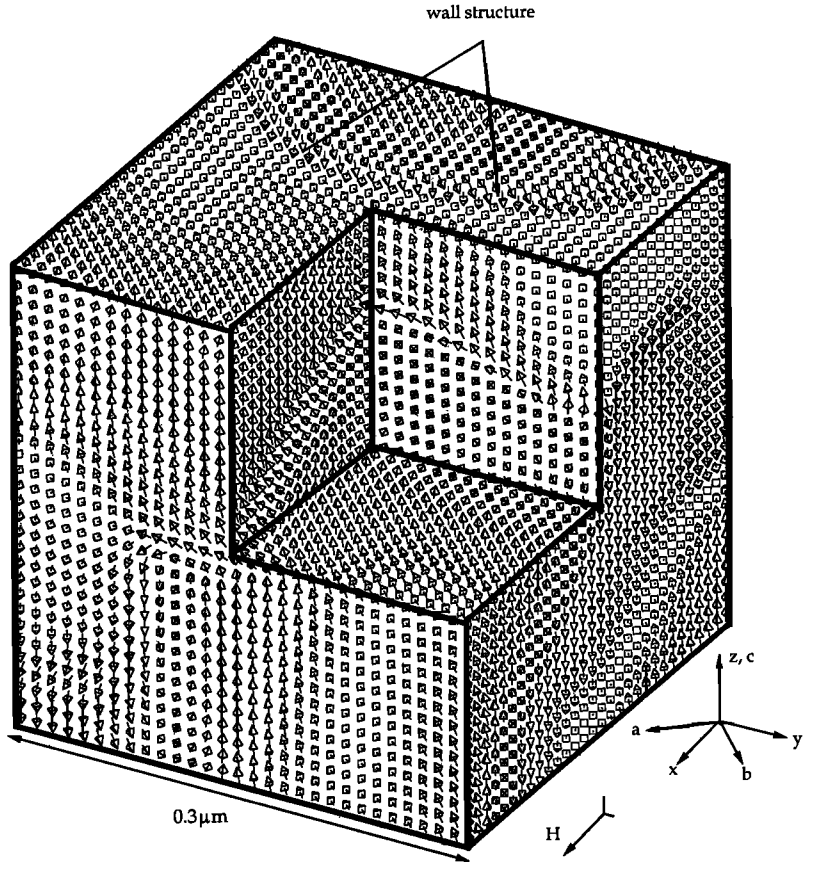

Figure 12. The domain structure of 0.3μm cubic grain of magnetite at 117 K, induced with a $SIRM_x$ at 270 K. The model resolution is 30 × 30 × 30. On cooling through T_v, the large increase in the magnetocrystalline anisotropy causes the magnetic vectors to lie in the a-plane, and the magnetization becomes more MD like.

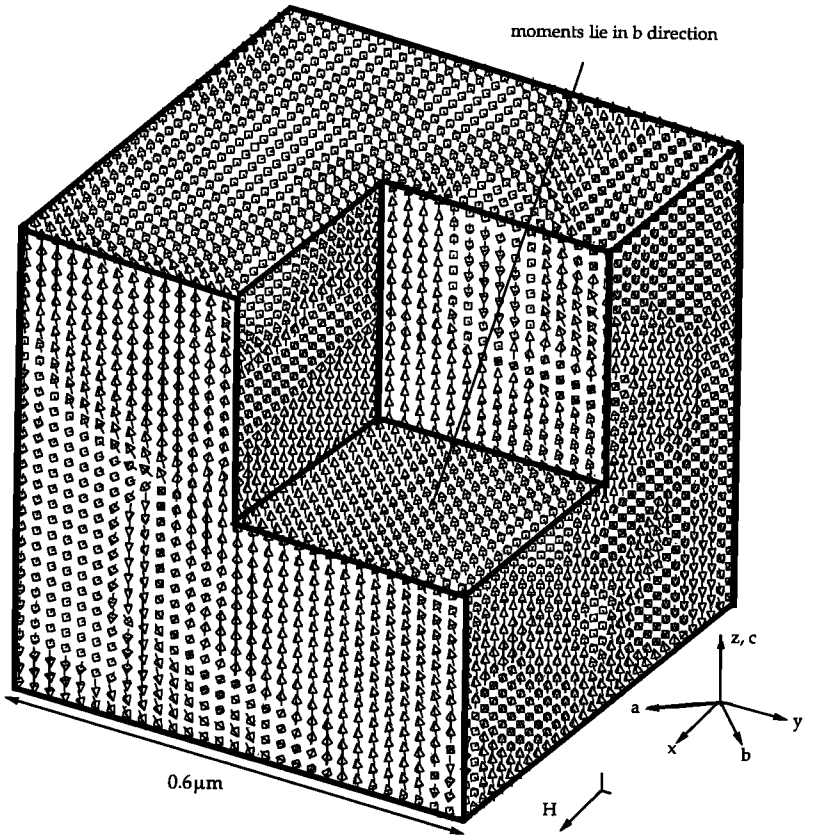

Figure 13. The domain structure of 0.6μm cubic grain of magnetite at 117 K, induced with a $SIRM_x$ at 270 K. The model resolution is 30 × 30 × 30. On cooling through T_v, the large increase in the magnetocrystalline anisotropy causes the magnetic vectors to lie in the a-plane, and the magnetization becomes more MD like. The direction of the inducing field is shown.

for both cases. The net effect of the low-temperature cycling of SIRM in 0.1 μm cubic grains is to align the magnetic moment in the direction of the monoclinic c axis (z axis).

5.1.2. The 0.3 μm cubic grains. The initial domain structure consists of a central body domain with four large domains at each corner which can be thought of as very large closure domains. The central body domain is partially aligned in the direction of the magnetocrystalline anisotropy easy axis, i.e., [111], but the net magnetization of both SIRMs is misaligned from the inducing field by $\leq 5°$. For an unknown reason the reduced magnetization of the $SIRM_x$ is half the intensity of $SIRM_z$ (Table 1).

On cooling from room temperature to above T_v the basic domain structure remains with only a small increase in the size of closure domains. The domain structure is relatively unchanged on cooling through T_k. On cooling through T_v the magnetic moments rotate away from the a direction, causing large changes to domain structure. The body domain of the initial $SIRM_z$ is aligned near the c direction and is relatively unaffected, but the large closure domains are reduced (Figure 12). The reduced efficiency of the closure domain and the rotation of magnetic vectors away from the direction of the a axis cause the net magnetization to increase and to lie close to or in the a plane (Table 1).

The body domain of the $SIRM_x$ in the cubic phase is aligned at only 45° from the hard a axis and on cooling through T_v rotates toward the c axis, in a similar manner to 0.1 μm $SIRM_x$. The closure domains similarly rotate, and the net magnetization is aligned at 54° from the c axis (Table 1). For both $SIRM_x$ and $SIRM_z$ in the monoclinic phase the closure domains partially join to give a domain structure similar to *Kittel*'s [1949] classic three-domain structure.

On warming back through T_v, $SIRM_z$ forms a "double-vortex" structure, that is, two vortices at either end of the grain rotating in opposite directions, similar to double vortices reported for elongated grains [*Fabian et al.*, 1996]. The net magnetization is reduced, however it retains a "memory" of its original orientation and rotates back toward this direction (Table 1). The $SIRM_x$ forms a single-vortex structure, which travels from a (010) plane to a (001) plane.

5.1.3. The 0.6 μm cubic grains. The initial remanences $SIRM_x$ and $SIRM_z$ both have domain structures which are slightly more complicated than vortex structure shown in Figure 5c and are partially aligned in the direction of the easy magnetocrystalline anisotropy

Table 2. Intensity and Direction of Simulated Reduced $TRM^{T_c}_{rtp}$, $pTRM^{T_c}_{477}$ and $pTRM^{477}_{rtp}$ During Low-Temperature Cycling for 0.1-0.6 μm Cubic Grains

Remanence	Initial		Monoclinic		Memory	
	M/M_{SD}	θ, ϕ	M/M_{SD}	θ, ϕ	M/M_{SD}	θ, ϕ
			0.1 μm			
$TRM^{T_c}_{rtp}$	0.91	90°, 0°	0.95	15°, 224°	0.92	6°, 225°
$pTRM^{T_c}_{477}$	0.92	90°, 0°	0.96	14°, 224°	0.92	4°, 225°
$pTRM^{477}_{rtp}$	0.92	90°, 0°	0.93	21°, 225°	0.92	14°, 228°
			0.3 μm			
$TRM^{T_c}_{rtp}$	0.03	90°, 359°	0.39	43°, 350°	0.003	83°, 6°
$pTRM^{T_c}_{477}$	0.04	90°, 337°	0.26	56°, 350°	0.007	88°, 331°
$pTRM^{477}_{rtp}$	0.02	91°, 357°	0.35	41°, 348°	0.03	83°, 0°
			0.6 μm			
$TRM^{T_c}_{rtp}$	0.02	90°, 351°	0.11	63°, 347°	0.01	93°, 351°
$pTRM^{T_c}_{477}$	0.03	93°,358°	0.03	18°,178°	0.01	1°,3°

The thermoremanences were induced in the x-direction.

axis (Table 1). The initial reduced remanences are of the order 0.01 (Table 1), in agreement with previous calculations of *Williams and Wright* [1998]. Unlike the smaller grain sizes, there are significant changes in the domain structure during simulated cooling from room temperature to T_v.

On cooling below T_v the domain structure changes radically, the magnetic moments aligning away from the a axis. In behavior similar to the other grain sizes, $SIRM_x$ rotates toward the c, z axis ($\theta = 44°$), while $SIRM_z$ is rotated away from the z axis ($\theta = 37°$) (Figure 13). There is increased leakage of magnetization, and the net remanence increases. There are a few discontinuities in the domain structure, i.e., 180° jumps in neighboring subcell orientations, and it is debatable as to how accurate a resolution of 30 × 30 × 30 is at modeling the domain structure below T_v. Calculations by *Muxworthy and Williams* [1999] suggest that the resolutions used to model the 0.1 μm grain size was sufficient, the 0.3 μm needed a slightly higher resolution but the model should still display the same trends, and a higher resolution is required to accurately model the 0.6 μm, though, again the model should still display the same trends.

On warming back through T_v, both $SIRM_x$ and $SIRM_z$ become simple vortex structures. The small reduced remanence returns to its original orientation and intensity (Table 1).

5.2. Behavior of Thermoremanences

Three different thermoremanence were induced in the x direction in three grain sizes 0.1 μm, 0.3 μm, and 0.6 μm; namely, a "full" thermoremanence $TRM^{T_c}_{rtp}$, a type 1 $pTRM^{T_c}_{477}$ and a type 2 $pTRM^{477}_{rtp}$. The thermoremanences were induced in one direction because of limitations on CPU time. The x direction was chosen over the z direction because such remanence domain structures were expected to display greater changes on cooling through T_v. In accordance with convention, both T_1 and T_2 in $pTRM^{T_1}_{T_2}$ are given in degrees Celsius.

5.2.1. The 0.1 μm cubic grains. The thermoremanence domain structures of 0.1 μm cubic grains at room temperature were flower states, similar to that of $SIRM_x$. Consequently, the low-temperature behavior did not vary significantly from $SIRM_x$. On cooling to below T_v the domain structures rotate toward the z axis until θ = 14–21°, with the small component in the z plane aligned in the b direction. On warming to 270 K the magnetic moments rotate back toward the x axis until θ = 4–14°, but there is also partial alignment with the magnetocrystalline anisotropy easy axis, i.e., $\phi \approx 225°$ (Table 2). There are differences in detail; the angle of the net magnetization is dependent of the type of thermoremanence; for example, $pTRM^{T_c}_{477}$ memory ($\theta = 4°$) is closer to the z axis than $pTRM^{477}_{rtp}$ memory ($\theta = 14°$).

5.2.2. The 0.3 μm cubic grains. All three thermoremanences display simple vortex structures, which are slightly antisymmetric to accommodate the small net remanence. The orientation of the vortex path depends on the type of thermoremanence. Simulated $TRM^{T_c}_{rtp}$ and $pTRM^{T_c}_{477}$ both have central vortex paths in the x direction, whilst the $pTRM^{477}_{rtp}$ vortex path is aligned in the y direction.

On cooling through T_v the vortex states of the three thermoremanences all form structures which resemble *Kittel's* [1949] two-domain structure. There is an increase in the magnetic flux leakage, and the reduced remanence increases for all three thermoremanences. The $pTRM^{477}_{rtp}$ moment is seen to be "weaker" because it rotates furthest from the x direction on cooling through the Verwey transition (Table 2). On warming to room temperature the vortex structure is recovered, but with a higher degree of symmetry than before cooling, decreasing the reduced magnetization.

5.2.3. The 0.6 μm cubic grains. The initial $TRM^{T_c}_{rtp}$ and $pTRM^{477}_{rtp}$ domain structures at 270 K have simple MD structures, with the magnetic structure in the cen-

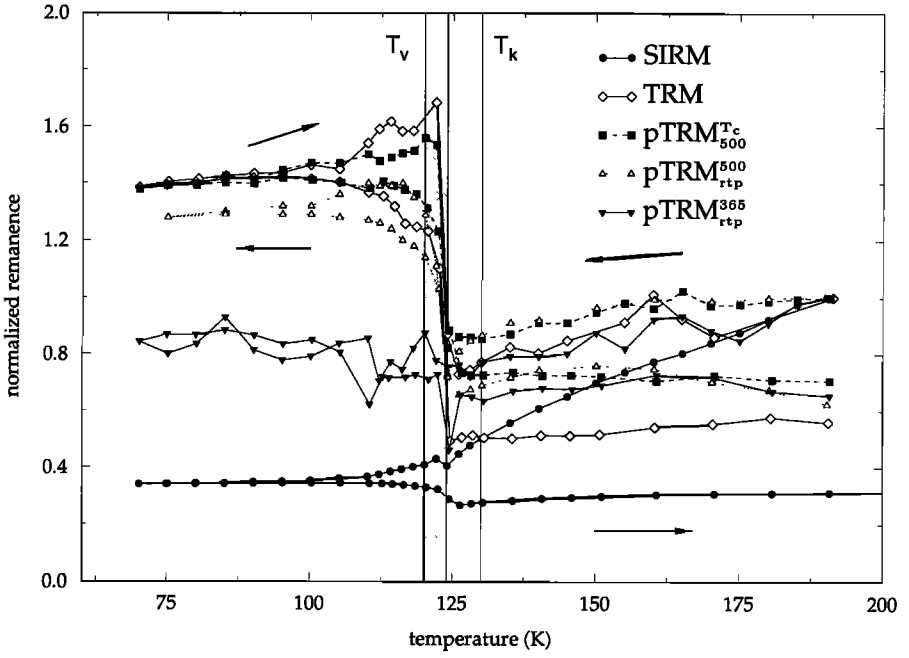

Figure 14. Simulated low-temperature cycling of different initial thermoremanences and $SIRM_x$ induced in a single 0.3μm cube. $SIRM_x$ rather than $SIRM_z$ is shown, because all the thermoremanences were induced in the x-direction. The remanence is normalized at 190 K.

ter of grain partially aligned in the direction of the easy magnetocrystalline anisotropy axis. The reduced magnetization of all three thermoremanences is very low, but the net remanences are closely aligned to the direction of the inducing field (Table 2). On cooling through T_v the net magnetization increases and rotates away from the direction of the applied field toward the monoclinic c-axis. The degree of rotation, i.e., the rotation of θ, is related to the initial thermoremanence; $pTRM^{477}_{rtp} > TRM^{T_c}_{rtp}$ (Table 2). $TRM^{T_c}_{rtp}$ has a greater intensity than $pTRM^{477}_{rtp}$ (Table 2).

On subsequent warming to room temperature, both $TRM^{T_c}_{rtp}$ and $pTRM^{T_c}_{477}$ become vortex states, with central vortex paths approximately in the [100] and [010] directions, respectively. The net magnetizations partially return to the original orientations; however, the intensities are reduced (Table 2).

6. Comparison With Experimental Results

Because the grain size under consideration, i.e., $\leq$ 0.6 μm, is less than the lower limit of domain observation [*Pokhil and Moskowitz*, 1997], direct comparisons with observational data cannot be made. However, the simulated low-temperature behavior of remanent magnetization and the magnetic memory ratio, i.e., the ratio of (remanence memory/remanence), can be compared with experimental results from the literature. The model in this paper considered only dislocation-free magnetite cubes; because of this it is preferable to consider experimental results from synthetic samples prepared by hydrothermal recrystallization which are know to have exceptionally low-internal dislocation densities [*Heider et al.*, 1988].

6.1. Remanent Magnetization Versus Temperature

The simulated low-temperature cycling results for a 0.3 μm cubic grain is shown in Figure 14. To our knowledge the most reliable set of low-temperature cycling results for a PSD hydrothermal sample induced with both TRM and SIRM is by *Muxworthy* [1998] and *Muxworthy and McClelland* [1999a] for an assemblage of randomly oriented crystals with mean grain size 7.5 μm (σ = 3.0 μm) (Figure 15). Although the hydrothermal sample size is larger than the model grain size, its SIRM thermomagnetic curve (Figure 15) is typical for small MD grains in the range 0.1–10 μm [e.g., *Halgedahl and Jarrard*, 1995; *King*, 1996].

There is rough agreement between the experimental trends and simulated low-temperature cycling behavior (Figures 14 and 15). The model confirms the relative behavior of the SIRM and thermoremanences; that is, the thermoremanences have larger anomalies at T_v, in agreement with the experimental results. However, the model SIRM displays a significant anomaly at T_v, whereas the experimental curve does not. This maybe due the inaccuracy of comparing assemblages of crystals with calculations for a single crystal. In an independent study, *Özdemir and Dunlop* [1999] have demonstrated the importance of orientation of SIRM; they found that an SIRM induced along the [001] direction of a single natural crystal displayed a significant reversible anomaly at T_v (Figure 16). Yet when

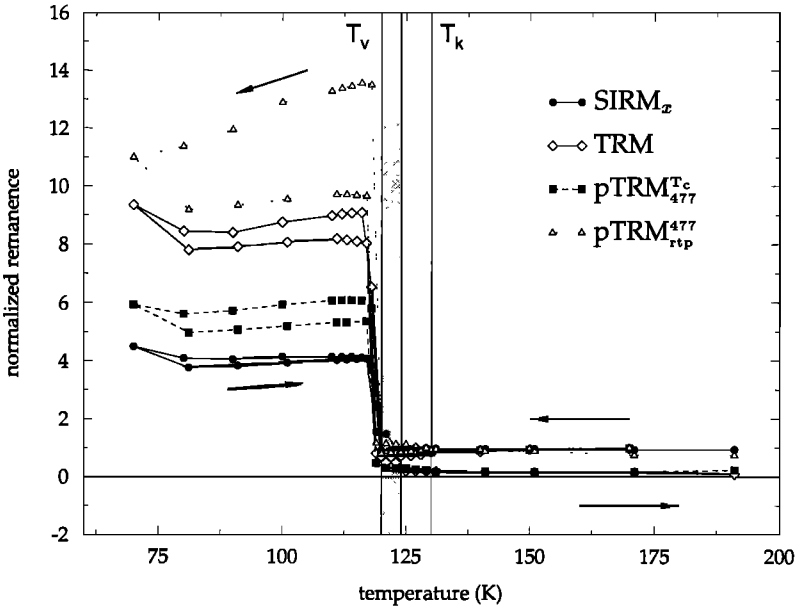

Figure 15. Low-temperature cycling of different initial thermoremanences induced in a hydrothermal sample with mean grain size 7.5 μm, containing an assemblage of randomly orientated crystals dispersed in vacuum sealed in quartz capsules. The remanence is normalized at 190 K. After *Muxworthy [1998]* and *Muxworthy and McClelland [1999]*.

the field was randomly orientated, the anomaly at T_v was greatly reduced, and the thermomagnetic curves displayed behavior similar to studies on randomly orientated assemblages [e.g., *Halgedahl and Jarrard*, 1995; *Hodych et al.*, 1998]. Clearly, caution should be used when comparing the results of 1.5 mm (octahedral) single crystal with those for a 0.3 μm grain; however, the model confirms the large reversible discontinuity in the magnetization observed on heating/cooling single crystals through T_v.

There are also differences in the thermoremanence curves. The modeled type 2 pTRM, i.e., pTRM$^{477}_{rtp}$, has a bigger anomaly than the type 1 pTRM pTRM$^{T_c}_{477}$ (Figure 14), in disagreement with the experimental results which found that type 2 pTRM, e.g., pTRM$^{500}_{rtp}$, has a smaller discontinuity at T_v than type 1 pTRM, e.g., pTRM$^{T_c}_{500}$ (Figure 15). This discrepancy may be a fault of the program, as the model takes several temperature steps to optimize the monoclinic domain structure; compare the decrease in the magnetization of pTRM$^{477}_{rtp}$ on cooling from T_v to 70 K (Figure 14). Other differences in behavior may be attributed to model simplifications; for example, the model did not include the effect thermal fluctuations, magnetostrictive anisotropy, and crystal defects and, in comparing results from assemblages, randomly orientated grains with the model calculations for single crystals.

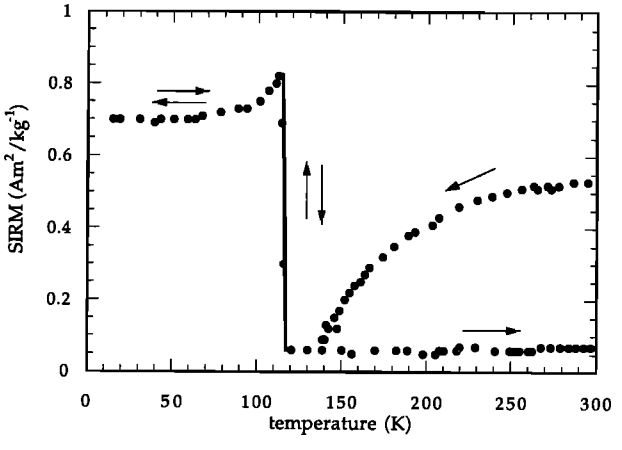

Figure 16. Low-temperature cycling of room-temperature SIRM induced in a natural crystal in a field of 2.5 T, orientated along the [001] axis. The natural crystal was a "museum-quality" 1.5 mm octahedral crystal. After *Özdemir and Dunlop [1999]*.

6.2. Magnetic Memory

Taking the average of the modeled memory ratios SIRM$_x$ and SIRM$_z$ to give an equivalent average SIRM for an assemblage of crystals, this is compared with experimental results in Figure 17. The average SIRM is in reasonably good agreement with the experimental results (Figure 17); the memory ratios for 0.1 μm and 0.3 μm cubes are slightly lower than the experimental results of *Dunlop and Argyle* [1991]. Differences maybe due to the lack of dislocations within the model, and because the method of estimating the average SIRM memory was crude. The modeled SIRM memory ratio for 0.6 μm is slightly higher than for the 0.1 μm and 0.3 μm cubes; however, it is suspected this is due to errors associated with modeling the monoclinic domain structure with a resolution of only 30 × 30 × 30.

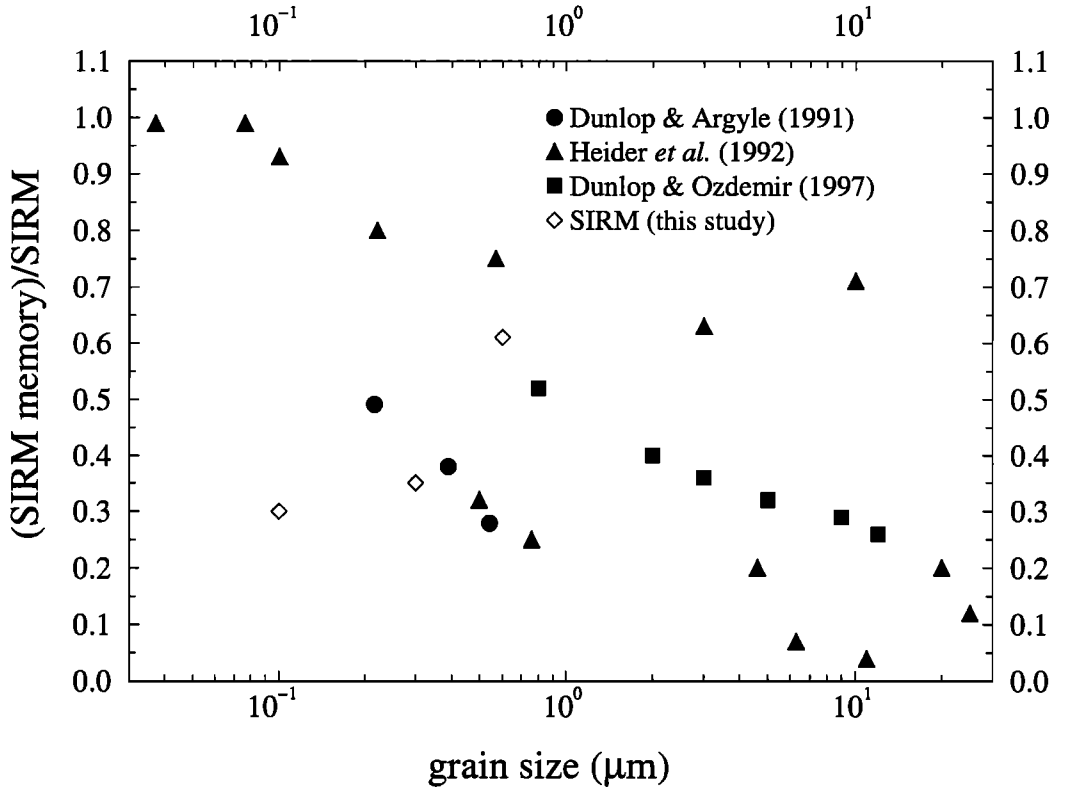

Figure 17. Low-temperature memory ratios for SIRM; representative experimental results are represented by closed symbols and the model results by an open.

7. Discussion

The general features of the results can be attributed to the large increase in the magnetocrystalline anisotropy on cooling through T_v. The large increase in the anisotropy increases the SD-critical size from 0.07 μm to 0.14 μm on cooling through T_v (Figure 8) and gives rise to the anomalous behavior of remanence during low-temperature cycling.

The behavior of SIRMs and thermoremanences to low-temperature cycling is revealing. For the smallest grain size, i.e., 0.1 μm, the behavior of SIRM and thermoremanences is dominated by the switching of the flower structure to the easy c axis. On repeating the $SIRM_x$ low-temperature cycling experiment for a 0.05 μm cube, it was found that the flower state rotates to align in the b axis, rather than the easier c axis on cooling through T_v. It would appear that there is some critical elongation and/or grain size where the shape anisotropy dominates the anisotropy, and suppresses the rotation from the cubic [100] direction to the monoclinic c axis. For the larger models, i.e., 0.3 μm and 0.6 μm, SIRM and thermoremanence rotate from the cubic orientation on cooling through T_v, with partial reversibility. The orientation of SIRM displays a greater recovery than thermoremanence on warming to room temperature; however, the memory ratio of SIRM is lower than that of thermoremanence because the SIRM domain structures rearrange to reduce the magnetic flux leakage. The difference in memory ratio suggests that SIRM is intrinsically weaker than TRM. Similarly, the ability to recover the original orientation on cycling through T_v suggests the TRM is trapped in a deeper, more flexible LEM states than $pTRM^{477}_{rtp}$. The large positive anomalies in all the remanences at T_v are attributed to the partially reversible reduction in closure domain-type structures.

7.1. Suitability of the Low-Temperature Demagnetization Technique

The technique of low-temperature demagnetization (LTD) has long been suggested in paleomagnetism as a technique of preferentially removing unwanted "soft" remanence of supposedly secondary origin [e.g., *Ozima et al.*, 1964; *Kobayashi and Fuller*, 1968]. In terms of using LTD as a means of removing MD remanence or soft remanence the model supports the idea that LTD preferentially demagnetizes weak domain structures or secondary remanences; for example, SIRM structures display a greater degree of reorganization than thermoremanence structures during LTD.

It has been suggested that the cause of LTD is due to cooling through either T_k, T_v or both [*Halgedahl and Jarrard*, 1995; *King*, 1996; *Shcherbakova et al.*, 1996; *Hodych et al.*, 1998]. The results from this model suggest

that the demagnetization occurs on cycling through T_v not T_k. The model also supports recent experimental studies [*Muxworthy and McClelland*, 1999a; *Özdemir and Dunlop*, 1999] that show that there are large discontinuities at T_v which are partially reversible and are dependent on remanence type and orientation. It is unclear as to the exact relationship between reversibility and demagnetization at T_v; however, it appears that thermoremanence structures (especially thermoremanence acquired at high temperatures) are better suited at retaining a record of their original magnetization after LTD and display larger reversible anomalies at T_v. The implication being that grains which display large anomalies at T_v are carrying stable remanence of a primary thermoremanent origin. The grain sizes considered in this model are too small to comment on whether the origin of large multidomain grains' memory is due to SD-like inclusions or or metastable MD structures [e.g., *Shcherbakova et al.*, 1996; *Özdemir and Dunlop*, 1998].

7.2. Consideration for Future Models

This model assumes that during the phase change from cubic to monoclinic at T_v and that all areas of a grain are orientated in the same direction; however, this is unlikely to be the case as experimental evidence has shown that a variety of twin-domain structures occur [*Otsuka and Sato*, 1986; *Medrano et al.*, 1999]. It has been suggested [*Moloni et al.*, 1996], that the twin domains in the monoclinic phase are magnetically independent; that is, the grain behaves magnetically like a polycrystal. However, this is unlikely to be the case as twin-domain walls have been shown to move easily in an external field [*Otsuka and Sato*, 1986]. Recently, *Medrano et al.* [1999] suggested that twin-domain walls may arrange themselves in an attempt to decrease the magnetostatic energy. It would appear therefore that to accurately model the low-temperature domain structure, it is necessary to incorporate the twin-domain structures into the model. However, at present, it is uncertain how large the interaction is. The absence of this maybe contributory to the discrepancies between the model in this paper and experimental results.

8. Conclusions

Our models of the low-temperature phase of magnetite have found that the SD critical size increases on cooling through T_v from 0.07 μm to 0.14 μm. The increase in grain size is attributed to the large increase in the magnetocrystalline anisotropy on cooling through T_v. However, it is postulated, that vortex structures in grains in the size range 0.07-0.14 μm will not denucleate domain walls on cooling through $T_v$because of the high-energy barriers involved; $\approx 5\times$ higher than room temperature barriers.

Simulations of low-temperature cycling display trends that are in rough agreement with experimental studies. The low-temperature behavior of remanence is found to be strongly controlled by the change in the magnetocrystalline anisotropy and by the orientation of the magnetization with respect to the monoclinic c axis. Central body domain structures are found to rotate toward the c axis on cooling through T_v, while energetically unfavorable closure domain structures are destroyed. The removal of the closure domains gives rise to increased remanence and a corresponding anomaly in the thermomagnetic low-temperature curve. The orientation of the larger central body domains was found to be partially reversible on heating back through T_v. Closure domains correspondingly return, giving rise to a large reversible anomaly at T_v, in agreement with recent experimental observations. The low-temperature simulations of various initial remanences display similar relationships to experimental results; that is thermoremanences display larger anomalies at T_v than SIRM. There is no evidence from the models to suggest that T_k controls the demagnetization process during low-temperature cycling.

Acknowledgments. We thank E. McClelland for const -ructive comments and V. Shcherbakov, M. Prevot and an anonymous reviewer for helpful reviews.

References

Abe, K., Y. Miyamoto, and S. Chikazumi, Magnetocrystalline anisotropy of low-temperature phase of magnetite, *J. Phys. Soc. Jpn.*, *41*(6), 1894–1902, 1976.

Belov, K., Electronic processes in magnetite (or "enigmas in magnetite"), *Physics Uspekhi*, *36*(5), 380–391, 1993.

Bickford, L., J. Brownlow, and R. F. Penoyer, Magnetocrystalline anisotropy in cobalt-substituted magnetic single crystals, *Proc. Inst. Electr. Eng.*, *B104*, 238–244, 1957.

Dunlop, D., and K. Argyle, Separating multidomain and single-domain-like remanences in pseudo-single-domain magnetites (215-540 nm) by low-temperature demagnetization, *J. Geophys. Res.*, *96*(B2), 2007–2017, 1991.

Dunlop, D., and O. Özdemir, *Rock Magnetism: Fundamentals and Frontiers*, Cambridge Univ, Press, New York, 1997.

Enkin, R., and W. Williams, Three-dimensional micromagnetic analysis of stability in fine magnetic grains, *J. Geophys. Res.*, *99*(B1), 611–618, 1994.

Fabian, K., and F. Heider, How to include magnetostriction in micromagnetic models of titanomagnetite grains, *Geophys. Res. Lett.*, *23*(20), 2839–2842, 1996.

Fabian, K., A. Kirchner, W. Williams, F. Heider, T. Leibl, and A. Hubert, Three-dimensional micromagnetic calculations for magnetite using fft, *Geophys. J. Int.*, *124*, 89–104, 1996.

Fletcher, E., and W. O'Reilly, Contribution of Fe^{2+} ions to the magnetocrystalline anisotropy constant K_1 of $Fe_{3-x}Ti_xO_4$ ($0 < x < 0.1$), *J. Phys. B: Solid State Phys.*, *7*, 171–178, 1974.

Halgedahl, S., and R. Jarrard, Low temperature behaviour of single domain through multidomain magnetite, *Earth Planet. Sci. Lett.*, *130*, 127–139, 1995.

Heider, F., and W. Williams, Note of temperature dependence of exchange constant in magnetite, *Geophys. Res. Lett.*, *15*(2), 184–187, 1988.

Heider, F., D. Dunlop, and N. Sugiura, Magnetic properties of hydrothermally recrystallised magnetite crystals, *Science*, *236*, 1287–1290, 1988.

Heider, F., D. Dunlop, and H. Soffel, Low temperature and

alternating field demagnetization of saturation remanence and thermoremanence in magnetite grains (0.037 μm to 5 mm), *J. Geophys. Res.*, *97*(B6), 9371–9381, 1992.

Hodych, J., Low-temperature demagnetisation of saturation remanence in rocks bearing multidomain magnetite, *Phys. Earth Planet. Inter.*, *66*, 144–152, 1991.

Hodych, J., R. Mackay, and G. English, Low-temperature demagnetization of saturation remanence in magnetite-bearing dolerites of high coercivity, *Geophys. J. Int.*, *132*, 401–411, 1998.

King, J., Magnetic properties of arrays of magnetite particles produced by the method of electron beam lithography (EBL), Ph.D. thesis, Univ. of Edinburgh, Edinburgh, Scotland, 1996.

Kittel, C., Physical theory of ferromagnetic domains, *Rev. of Mod. Phys.*, *21*(4), 541–583, 1949.

Kobayashi, K., and M. Fuller, Stable remanence and memory of multidomain materials with special reference to magnetite, *Philos. Mag.*, *18*, 601–624, 1968.

McClelland, E., and V. Shcherbakov, Metastability of domain state in MD magnetite: Consequences for remanence acquisition, *J. Geophys. Res.*, *100*(B3), 3841–3857, 1995.

Medrano, C., M. Schlenker, J. Baruchel, J. Espeso, and Y. Miyamoto, Domains in the low-temperature phase of magnetite from synchroton-radiation x-ray topographs, *Phys. Rev. B Condens. Matter*, *59*, 1185–1195, 1999.

Moloni, K., B. Moskowitz, and E. Dahlberg, Domain structures in single crystal magnetite below the Verwey transition as observed with a low-temperature magnetic force microscope, *Geophys. Res. Lett.*, *23*(20), 2851–2854, 1996.

Moskowitz, B., High-temperature magnetostriction of magnetite and titanomagnetites, *J. Geophys. Res.*, *98*(B1), 359–371, 1993.

Muxworthy, A., Stability of magnetic remanence in multidomain magnetite, Ph.D. thesis, Univ. of Oxford, Oxford, England, 1998.

Muxworthy, A., and E. McClelland, The causes of low-temperature demagnetisation of remanence in multidomain magnetite, *Geophys. J. Int.*, in press, 1999a.

Muxworthy, A., and E. McClelland, Review of the low-temperature magnetic properties of magnetite from a rock magnetic perspective, *Geophys. J. Int.*, in press, 1999b.

Muxworthy, A., and W. Williams, Micromagnetic calculation of coercive force as a function of temperature in pseudo-single domain magnetite, *Geophys. Res. Lett.*, *26*(8), 1065–1068, 1999.

Néel, L., Propriétés d'un ferromagnétique cubique en grain fins., *C. R. Acad. Sci.*, *224*, 1488–1490, 1947.

Otsuka, N., and H. Sato, Observation of the Verwey transition in Fe_3O_4 by high-resolution electron microscopy, *J. Solid. State Chem.*, *61*, 212–222, 1986.

Özdemir, O., and D. Dunlop, Single-domain-like behavior in a 3-mm natural single crystal of magnetite, *J. Geophys. Res.*, *103*(B2), 2549–2562, 1998.

Özdemir, O., and D. Dunlop, Low-temperature properties of a single crystal of magnetite orientated along principal magnetic axes, *Earth Planet. Sci. Lett.*, *165*, 229–239, 1999.

Ozima, M., M. Ozima, and T. Nagata, Low-temperature treatment as an effective means of "magnetic cleaning" of natural remanent magnetisation., *J. Geomagn. Geoelectr.*, *16*, 37–41, 1964.

Pauthenet, R., and L. Bochirol, Aimantation spontanée des ferrites, *J. Phys. Radium*, *12*, 249–251, 1951.

Pokhil, T., and B. Moskowitz, Magnetic domains and domain walls in pseudo-single-domain magnetite studied with magnetic force microscopy, *J. Geophys. Res.*, *102*(B10), 22,681–22,694, 1997.

Rave, W., K. Fabian, and A. Hubert, The magnetic states of small cubic magnetic particles with uniaxial anisotropy, *J. Magn. Magn. Mater.*, *190*, 332–348, 1998.

Schmidbauer, E., and R. Keller, Magnetic properties and rotational hysteresis of Fe_3O_4 and γ-Fe_2O_3 particles ~ 250 nm in diameter, *J. Magn. Magn. Mater.*, *152*, 99–108, 1996.

Shcherbakova, V., V. Shcherbakov, P. Schmidt, and M. Prevot, On the effect of low-temperature demagnetisation on trm and ptrms, *Geophys. J. Int.*, *127*, 379–386, 1996.

Thomson, L., R. Enkin, and W. Williams, Simulated annealing of three dimensional micromagnetic structures and simulated thermoremanent magnetization, *J. Geophys. Res.*, *99 (B1)*, 603–606, 1994.

Torrie, B., Spin-waves in magnetite at a temperature below the electronic ordering transition, *Solid State Commun.*, *5*, 715–717, 1967.

Tsuya, N., K. Arai, and K. Ohmori, Effect of magnetoelastic coupling on the anisotropy of magnetite below the transition temperature, *Physica B*, *86-88*, 959–961, 1977.

Verwey, E., Electronic conduction of magnetite (Fe_3O_4) and its transition point at low-temperature, *Nature*, *44*, 327–328, 1939.

Vinogradov, Y., and G. Markov, On the effect of low temperature heating on the domain state of multidomain magnetite, in *Investigations in rockmagnetism and palaeomagnetism* (in Russian), pp. 31–39, Inst. of Phys. of the Earth, Moscow, 1989.

Williams, W., and D. Dunlop, Three-dimensional micromagnetic modelling of ferromagnetic domain structure, *Nature*, *377*, 634–637, 1989.

Williams, W., and T. M. Wright, High-resolution micromagnetic models of fine grains of magnetite, *J. Geophys. Res.*, *103* (B12), 30,537-30,550, 1998.

Wright, T., W. Williams, and D. Dunlop, An improved algorithm for micromagnetics, *J. Geophys. Res.*, *102*(B6), 12,085–12,094, 1997.

Ye, J., A. Newell, and R. Merrill, A re-evaluation of the magnetocrystalline anisotropy and magnetostriction constants, *Geophys. Res. Lett.*, *21*(1), 25–28, 1994.

A.R. Muxworthy, Institut für Allgemeine und Angewandte Geophysik, Universität München, Theresienstrasse 41, D-8000 München, Germany. (adrian@rockmag.geophysik.uni-muenchen.de)

W. Williams, Department of Geology and Geophysics, University of Edinburgh, West Mains Road, Edinburgh EH9 3JZ, Scotland. (williams@glg.ed.ac.uk)

(Received November 20, 1998; revised June 17, 1999; accepted August 19, 1999.)